Effect of isotope mass on simulations of the high-mode pedestal and edge localized modes

Stacy E. Snyder, Arnold H. Kritz, and Glenn Bateman
Lehigh University, Department of Physics, 16 Memorial Drive East, Bethlehem, Pennsylvania 18015

Thawatchai Onjun
Sirindhorn International Institute of Technology, Klong Luang, Pathumthani 12121, Thailand

Vassili Parail and EFDA JET Contributors
Euratom/UKAEA, Fusion Association, Culham Science Centre, Abingdon, OX14 3DB, United Kingdom

(Received 28 July 2005; accepted 19 October 2005; published online 28 November 2005; publisher error corrected 19 May 2006)

Simulations of Joint European Torus (JET) [P. H. Rebut *et al.*, Nucl. Fusion **25**, 1011 (1985)] type I high-mode (H-mode) discharges with edge localized modes (ELMs) are used to study the effect of isotope mass on the height of the pedestal and the frequency of ELMs. A dynamic model for the H-mode pedestal and ELM cycles is employed in the JETTO integrated modeling code [M. Erba *et al.*, Plasma Phys. Control. Fusion **39**, 261 (1997)]. The stability criteria that are used to trigger ELM crashes in the JETTO simulations are calibrated with the HELENA and MISHKA ideal magnetohydrodynamic (MHD) stability codes [A. B. Mikhailovskii *et al.*, Plasma Phys. Rep. **23**, 713 (1997)]. Results obtained using a pedestal model in which the pedestal width increases with isotope mass are compared with those obtained using a fixed, prescribed pedestal width. In JET type I ELMy H-mode discharges, it is found that the height of the pressure pedestal increases and that the frequency of the ELMs decreases as the isotope mass is increased. Both of these experimentally observed trends are obtained simultaneously in the simulations only if the pedestal width increases with isotope mass. The physical processes that play a significant role in these simulations are described. © *2005 American Institute of Physics*. [DOI: 10.1063/1.2136352]

I. INTRODUCTION

Properties of high-mode (H-mode) discharges with edge localized modes (ELMs) in tokamaks make them a favorable starting point for the discharges that will be studied in the next generation of burning plasma devices such as ITER.[1–3] H-modes, or high confinement modes, first discovered in 1982 in the ASDEX tokamak,[4] produce a noticeable improvement in confinement over L-modes, or low-confinement modes. This improvement is the result of a transport barrier that forms near the edge of the plasma in H-mode discharges. This transport barrier results in a pedestal, which is a narrow region with steep gradients in the plasma temperature, density, and pressure profiles near the edge of the plasma.[5–9]

H-modes are usually accompanied by ELMs, which involve periodic losses of plasma that occur on a short time scale (on the order of or less than a millisecond) near the boundary of the plasma. Each ELM crash results in an avalanche-like burst of particles and energy at the edge of the plasma, along with a brief deterioration of plasma confinement. Despite the temporary reduction in confinement and the damage caused by energetic particles on the diverter, ELMs might be useful because they help to reduce the accumulation of impurities within the plasma. ELMs are believed to be caused by various magnetohydrodynamic (MHD) instabilities. The spatial structure of ELM crashes is consistent with the predictions of MHD instabilities, and ELM crashes occur on MHD time scales, which are much shorter than transport time scales. The ideal MHD instability model includes effects of the pressure gradient, current density, and magnetic shear, but does not directly involve isotope mass. Nonetheless, experimental results indicate that the isotope mass of the main plasma species does, at least indirectly, influence the H-mode pedestal and ELM properties.[6,10] A more complete understanding of the physical mechanisms involved in these effects should aid in the optimal use of ELMy H-mode discharges in future burning plasma devices.

Our objective in this work is to use predictive modeling simulations of plasma discharges to investigate the effect of isotope mass on the height and width of the H-mode pedestal and on the frequency of ELMs. In this study, the JETTO integrated modeling code[11] is used to predict the height of the pedestal as well as the frequency of the ELM crashes. The ideal MHD stability criteria that are used in the JETTO code to trigger ELM crashes are validated using the HELENA and MISHKA codes.[12] Quantitative comparisons are made with experimental data for the pressure at the top of the pedestal and for the frequency of ELMs.

In this paper, the details of the discharges examined are presented in Sec. II. A description of the JETTO transport code is provided in Sec. III, together with the specific conditions used for the simulations. The application of the MHD stability analysis is addressed in Sec. IV. The comparison of

[a]Appendix of J. Pamela *et al.*, Fusion Energy 2004, *Proceedings of the 20th International Conference*, Vilamoura, 2004 (IAEA, Vienna, 2004).

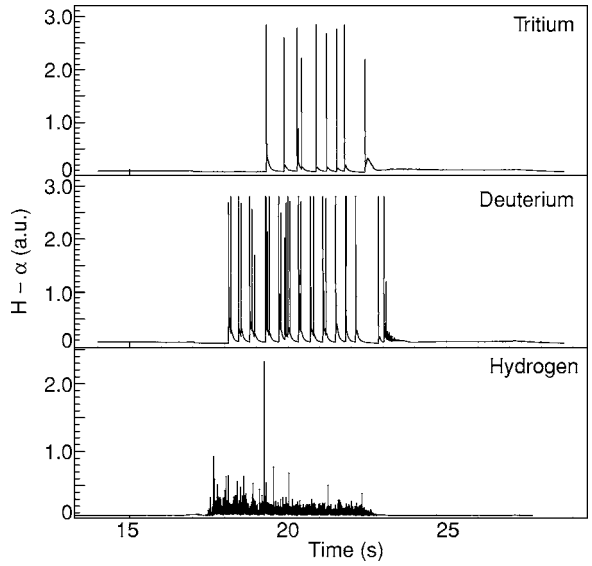

FIG. 1. The H-alpha signal vs time for the JET tritium discharge 43003, the deuterium discharge 43154, and the hydrogen discharge 43392.

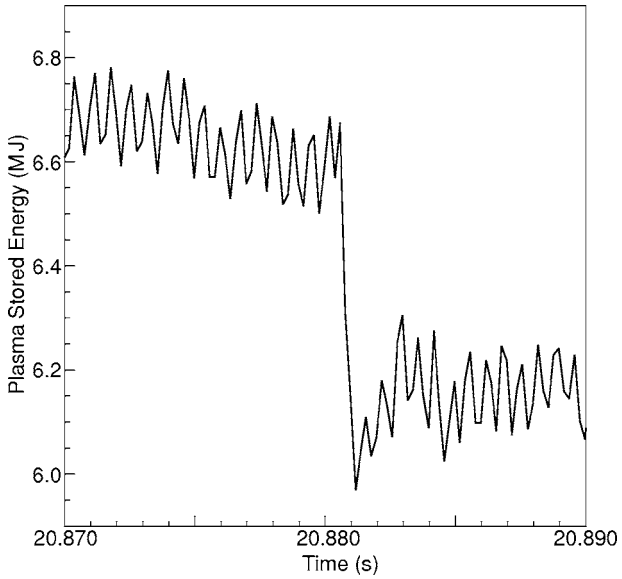

FIG. 2. Plasma stored energy vs time for the JET tritium discharge 43003. The decrease in stored energy during the ELM crash occurs during a time period of approximately 0.5 ms.

results with experimental data as well as a description of the physical phenomena observed in the simulations are contained in Sec. V.

II. EXPERIMENTAL DATA

The discharges considered for this study are derived from a JET isotope mass scan.[6] It was found in the JET discharges that the ELM frequency decreases and the pedestal height increases moderately with increasing isotope mass. The ELM frequency is obtained from the experimental H-alpha emission as a function of time, as shown in Fig. 1, for a pure tritium discharge (43003), a deuterium discharge (43154), and a hydrogen discharge (43392). The tritium and deuterium discharges exhibit type I or giant ELMs, which are characterized by a frequency that increases with heating power, whereas the hydrogen discharge, which has a lower density than the deuterium or tritium discharges, exhibits type III ELMs. Type III ELMs are smaller, with more frequent bursts, than type I ELMs, and type III ELMs are characterized by a frequency that decreases with heating power. For type I ELMs in JET, the typical loss of plasma energy resulting from each ELM crash is roughly 3%–10%. A specific instance of the loss of plasma stored energy during an ELM crash is shown in Fig. 2 for the tritium discharge.

In this study, simulations are carried out for the JET steady-state pure tritium (43003) and pure deuterium (43154) type I H-mode discharges. These discharges have similar values for the plasma current, toroidal magnetic field, and injected power, as shown in Table I. The notation used throughout this paper is also included in Table I. Both discharges have neutral beam heating and no gas fueling. A hydrogen discharge with similar density and with type I ELMs was not available.

The H-alpha signals for the pure tritium and deuterium discharges with an expanded time scale are shown in Fig. 3. Composite ELMs can be seen in the deuterium discharge, and, to a lesser extent, in the tritium discharge. Composite ELMs like those in Fig. 3 are often seen in the case of high recycling conditions with only one cryopump.[6] Different choices are possible when determining the experimental value for the frequency of ELMs. Open to question is whether all the spikes should be counted as separate ELM crashes, whether just the very high spikes should be counted, or whether each compound ELM should be counted as one ELM crash. If only type I ELM crashes are to be included, one possible method is to use the magnitude of the type III ELMs of the hydrogen shot (a maximum of 7×10^{14} for the H-alpha signal shown in Fig. 1 during the given time range) as a reference and to discard any spikes below this value. With this approach, it can be seen that the frequency of type I ELMs is lower for the discharge with higher isotope mass, i.e., it is lower for tritium than for deuterium.

The height of the pressure pedestal is found to increase moderately with isotope mass in the JET discharges considered. From the experimental data stored in the ITPA Pedestal Database[13] for the JET deuterium and tritium discharges studied, it is found that the height of the electron contribution to the pressure pedestal, that is, the value of the electron contribution to thermal pressure at the top of the edge transport barrier just before an ELM crash, is approximately 10 kPa for the deuterium discharge and 14 kPa for the tritium discharge. Previously it was shown that the increase in global H-mode plasma confinement with increasing isotope mass is a result of an increase in pedestal height with increasing isotope mass.[10]

III. THE JETTO INTEGRATED MODELING CODE

The one-and-one-half-dimensional ($1\frac{1}{2}$D) integrated predictive modeling code JETTO is used to simulate the evolution of current, temperature, and density profiles throughout the plasma, including both the core and the pedestal regions. The edge temperature and density boundary conditions are

TABLE I. Experimental data.

		Tokamak discharge isotope	JET 43154 deuterium	JET 43003 tritium
R	m	Major radius	2.90	2.90
a	m	Minor radius	0.92	0.92
κ	—	Elongation	1.83	1.84
δ	—	Triangularity	0.31	0.31
M_{eff}	amu	Effective mass of plasma	2.0	2.9
B_T	T	Toroidal magnetic field at geometric center	2.77	2.77
I_p	MA	Plasma current	2.57	2.58
n_{eo}	m^{-3}	Central electron density	8.04×10^{19}	7.75×10^{19}
n_e^{ped}	m^{-3}	Electron density at pedestal top before an ELM crash	6.3×10^{19}	6.3×10^{19}
Z_{eff}	—	Line average plasma effective charge (center)	2.2	3.2
P_{inj}	MW	Total injected NB power that passes into torus	11.0	10.5
P_{rad}	MW	Total radiated power	4.7	5.7
P_{ohm}	MW	Ohmic power	0.58	0.55
P_{tot}	MW	Total power input ($P_{\text{inj}}+P_{\text{ohm}}$)	11.6	11.1
p_e^{ped}	kPa	Electron pressure at pedestal top before an ELM crash	10	14
T_e^{ped}	keV	Electron temperature at pedestal top before ELM crash	0.98	1.3

imposed at the separatrix, which is at the base of the pedestal. Edge boundary values in the JETTO simulations are 20 eV for the electron and ion edge temperatures and 1.0×10^{13} m^{-3} for the electron density. Lönnroth has shown that JETTO simulation results are not sensitive to boundary conditions for type I ELMy H-mode plasmas whenever gas puffing is not large.[14] On the other hand, Onjun has found that ELM frequency decreases as the temperature at the separatrix is reduced.[15] A lower temperature at the boundary is associated with a higher edge resistivity and a faster removal of edge current density during and immediately after an ELM crash. Although the temperature boundary condition chosen may affect the ELM frequency somewhat, this effect does not prevent the comparison of simulations using different isotope masses. Onjun also notes that the temperature at the separatrix has little, if any, influence on the temperature and density at the top of the pedestal before an ELM crash or on the thermal energy content of the plasma.[15]

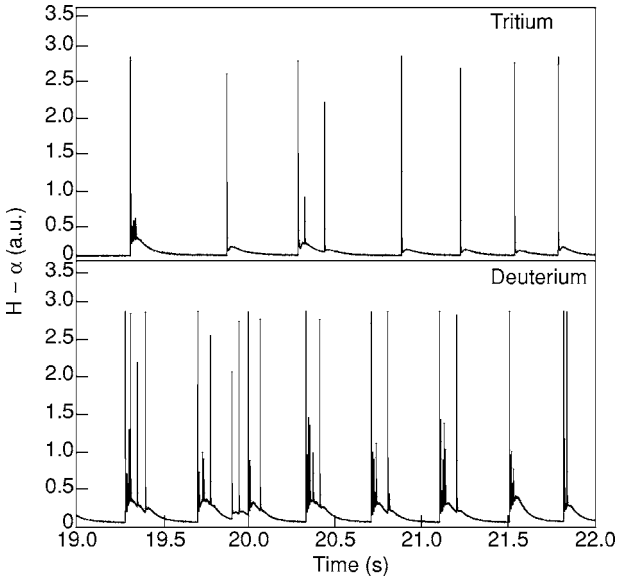

FIG. 3. The H-alpha signal vs time on an expanded time scale for the tritium discharge 43003 and the deuterium discharge 43154.

In the JETTO simulations, the core transport is computed using the JETTO mixed-Bohm/gyro-Bohm model[11] together with the NCLASS neoclassical transport model.[16] Information regarding these models is available in the NTCC module library.[17] It is assumed that turbulent transport is suppressed between the top of the pedestal and the separatrix between ELM crashes. Since the width of the pedestal is on the order of an ion banana width, transport is not expected to vary appreciably across the width of the pedestal. Therefore, the diffusivity throughout the edge transport barrier is set equal to the neoclassical diffusivity computed at the top of the pedestal. Consistent with the model used in previous publications,[8,9,14,18] the diffusion coefficients for all of the channels of transport (ion thermal, electron thermal, and particle) are set equal to the ion thermal neoclassical diffusivity computed at the top of the pedestal.

In the simulations, complete recycling is used together with a small negative amount of gas puffing to compensate for the neutral beam ion source and to ensure that the average electron density is approximately constant during the simulated two second time interval. For both the deuterium and tritium discharges, the plasma effective charge, Z_{eff}, is taken to have a radially uniform value of 2.1. Neutral beam heating and radiation power densities are taken from experimental analyses.

It is believed that ELMs are caused by MHD instabilities that are triggered either by a sufficiently large pressure gradient that results in a ballooning mode instability or by a sufficiently large current density that results in a kink or peeling mode instability. The JETTO simulations described in

this paper incorporate ELMs initiated by both ballooning and peeling modes. ELM crashes are triggered by a ballooning mode in the simulations when the normalized pressure gradient, α, is equal to or greater than a prescribed critical value, α_c, anywhere within the pedestal region. The normalized pressure gradient is given by

$$\alpha \equiv -\frac{2\mu_0 q^2}{\epsilon B_T^2}\frac{\partial p}{\partial \rho}, \tag{1}$$

where q is the safety factor, p is plasma pressure, ϵ is the inverse aspect ratio (minor radius divided by major radius), B_T is the toroidal magnetic field, and ρ is the normalized minor radial coordinate (half-width of the flux surface divided by the plasma minor radius). The value of the critical normalized pressure gradient, α_c, is determined by using the MHD stability analyses described in Sec. IV. ELM crashes are triggered by a peeling mode in the simulations whenever the parallel current density, $J_\parallel$, satisfies the condition

$$\sqrt{1-4D_M}+C<1+\frac{1}{\pi q'}\oint\frac{\mu_o J_\parallel B}{R^2 B_p^3}dl, \tag{2}$$

where D_M is the Mercier coefficient and where the constant C is the vacuum energy parameter.[19] For the simulations presented in this paper, a value of 0.2 was used for C. In Eq. (2), q' is the derivative of the safety factor with respect to poloidal flux, $J_\parallel$ is the current density parallel to the magnetic field, B_p is the poloidal component of the magnetic field B, R is the major radius, and dl is the poloidal arclength.

If the normalized pressure gradient α equals or exceeds α_c anywhere within the pedestal or if the condition given by Eq. (2) is met, the ion neoclassical thermal transport coefficients in the pedestal are enhanced by a factor of 300 for electrons and ions, and the particle transport coefficients are increased by a factor of 100 for a fixed time interval of 0.5 ms. Although the duration of an ELM crash varies in experiments, the 0.5 ms time interval is a typical ELM crash duration for JET type I ELMy discharges, as can be seen from the specific ELM crash shown in the plot of plasma stored energy versus time in Figure 2. Within the 0.5 ms interval of the simulated ELM crash, the transport is increased linearly during the first 0.1 ms of the crash, remains at its maximum level for the next 0.3 ms, and then decreases linearly for the remaining 0.1 ms of the crash. This sudden increase in transport results in a burst of plasma energy and particles escaping from the plasma. As a result, the pedestal pressure gradient and current density decrease during an ELM crash, and the plasma returns to a stable state with α below the critical value, α_c. The values used for the increased pedestal transport during the ELM crash are those used in previous publications[8,9,14,18] and are found to give simulation results that are consistent with ELM behavior in JET discharges.

No attempt is made in the JETTO simulations to reproduce details of the nonlinear dynamics during an ELM crash. The simulations are designed to provide realistic plasma profiles, both before and immediately after an ELM crash. In addition, the model is limited in its ability to reproduce the randomness of ELM crashes in experimental data,[20] along with the structure of the compound ELM crashes, as seen in Fig. 3.

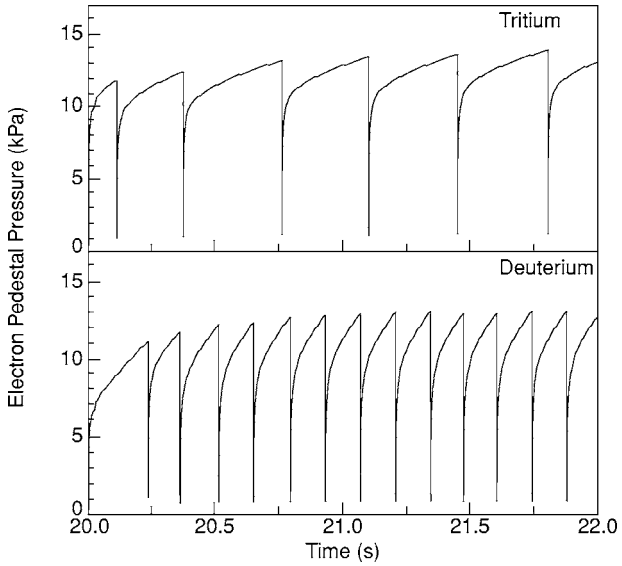

FIG. 4. Simulation results for the electron contribution to pedestal pressure vs time for the tritium and deuterium discharges when the pedestal width is taken proportional to the ion thermal Larmor radius. Parameters in the simulations are those appropriate for the JET tritium discharge 43003 and the JET deuterium discharge 43154, respectively.

A. JETTO simulations

The interpretation of the simulation results presented in this section will be presented in Sec. V. In the baseline simulations, the pedestal width in the deuterium discharge, Δ_D, is taken to be proportional to the deuterium ion thermal Larmor radius, ρ_D, and similarly, the pedestal width in the tritium discharge, Δ_T, is taken proportional to the tritium thermal ion Larmor radius, Δ_T.[21] Thus, the ratio of pedestal widths is given by

$$\frac{\Delta_T}{\Delta_D}=\frac{\rho_T^{th}}{\rho_D^{th}}=\frac{m_T v_T^{th}}{m_D v_D^{th}}=\sqrt{\frac{m_T T_T}{m_D T_D}}\cong 1.22\sqrt{\frac{T_T}{T_D}}, \tag{3}$$

assuming that the magnetic field B is the same for the tritium and deuterium discharges. Thus, for similar temperatures at the top of the pedestal, the pedestal width will be larger for tritium than for deuterium.

The critical normalized pressure gradient, α_c, used in each of the JETTO simulations is determined by stability analyses carried out using the HELENA and MISHKA codes, as described in Sec. IV. These analyses yield an approximate value of $\alpha_c=1.65$ for both the tritium and deuterium simulations. Results of the JETTO baseline simulations, where the pedestal width is proportional to the ion thermal Larmor radius, are shown in Fig. 4. The plot of simulated pedestal pressure versus time shows that the ELM frequency is significantly higher in the deuterium simulation (lower panel) than it is in the tritium simulation (upper panel). In the tritium simulation, all of the ELM crashes are triggered by ballooning modes. In the deuterium simulation, however, compound ELMs are observed in which an ELM crash triggered by a ballooning mode is typically followed immedi-

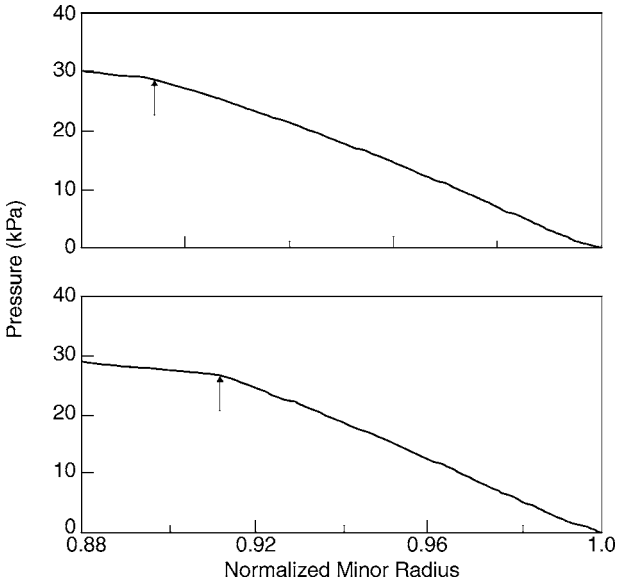

FIG. 5. Pressure pedestal as a function of the normalized minor radius near the edge of the plasma before and ELM crash for baseline simulations of the tritium discharge 43003 (top panel) and the deuterium discharge 43154 (bottom panel). Arrows indicate the pedestal tops.

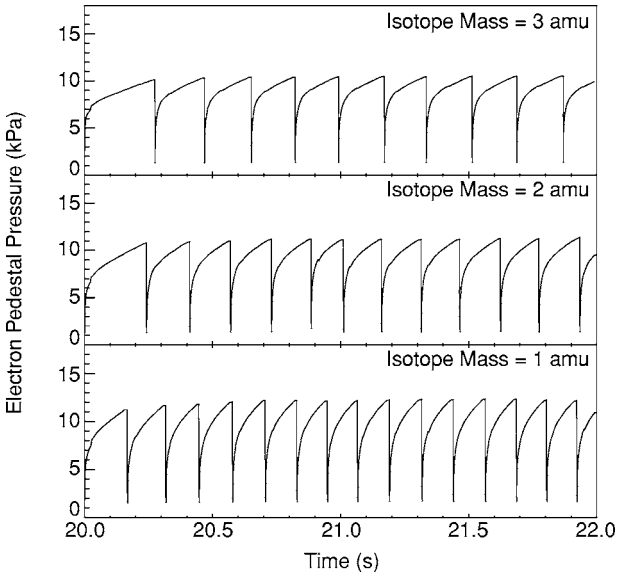

FIG. 6. Electron pedestal pressure vs time obtained in simulations in which pedestal width is fixed at 4.0 cm. Results are presented for tritium (top panel), deuterium (middle panel), and hydrogen (bottom panel).

ately by an ELM crash triggered by a peeling mode. (Note that the resolution in Fig. 4 is insufficient to show compound ELMs in the deuterium simulation.) The simulated electron pressure at the top of the pedestal varies somewhat with time, but the tritium pedestal electron pressure attains a slightly higher value than does the deuterium electron pedestal temperature. For the two second simulation shown in Fig. 4, the peak pressure at the top of the tritium barrier region is approximately 14 kPa, while for the deuterium simulation, the peak pedestal pressure is approximately 13 kPa.

As noted above, the ballooning mode instability, which is the initial cause of the ELM crashes in simulations of both the deuterium and tritium discharges, occurs when α exceeds α_c anywhere within the pedestal. It is found in the simulations that, as a consequence of the density profile, the pressure gradient varies in the pedestal region and that the condition for the ballooning mode instability is satisfied at a normalized minor radius of approximately 0.978 for tritium and 0.974 for deuterium. The arrows in Fig. 5 indicate the tops of the pedestals, which extend from $\rho=0.892$ to $\rho=1$ in the tritium simulation and extend from $\rho=0.910$ to $\rho=1$ in the deuterium simulation. Thus, ELM crashes are triggered at a location that is 20% of the pedestal width, measured in from the separatrix, in the tritium simulation, and 29% of the pedestal width from the separatrix in the deuterium simulation. It has been shown by Lönnroth *et al.*[22] that the ELM frequency decreases in JETTO simulations as the ELM perturbation is triggered farther from the edge of the plasma, as is found here when tritium simulations are compared with deuterium simulations. In his simulations, Lönnroth used a model that was more complicated than ours for the enhancement of transport during each ELM crash in order to account for changes in the width of the ELM crash in response to the location of the ELM trigger. However, the basic trend, that the ELM decreases as the ELM perturbation is triggered farther from the edge of the plasma, remains the same.

In the results presented in Figs. 4 and 5, it is seen that the ELM frequency and the pedestal height and width are different in the tritium and the deuterium simulations. In order to investigate how the isotope mass affects the H-mode pedestal and ELMs, simulations were carried out in which the pedestal width was held fixed while the isotope mass was varied. To keep conditions as similar as possible for simulations with different isotope mass, conditions from experimental data for the deuterium shot 43154 were used in both simulations. The width of the pedestal was fixed to 4 cm, the critical pressure gradient, α_c, was set to 1.65, and radiation was set to be radially constant. Only the ballooning mode instability criteria was used to initiate ELM crashes in these simulations.

The results of the simulations with fixed pedestal width are presented in Fig. 6. The ELM frequency is found to decrease with increasing isotope mass, which is similar to the trend observed in the experimental data. For isotope masses of 1, 2, and 3 amu, respective ELM frequencies were approximately 7.8, 6.2, and 5.3 Hz. However, in contrast to the trend observed in the experimental data, the electron pressure at the top of the barrier was found to decrease with increasing isotope mass when the simulations are carried out with a fixed isotope width. The simulated electron pedestal pressure for isotope masses of 1, 2, and 3 amu are approximately 12.3, 11.2, and 10.5 kPa, respectively. For consistency with the plots in Figs. 4 and 7, and for the ease of comparison with experimental data in the pedestal database, only the electron contribution to pressure is plotted in Fig. 6. The total pressure at the top of the pedestal shows the same trends.

In order to investigate the effect of changing only the pedestal width, simulations were carried out using a constant isotope mass of 2 amu and a constant α_c value of 1.65, but with two different pedestal widths. Beginning with the JET

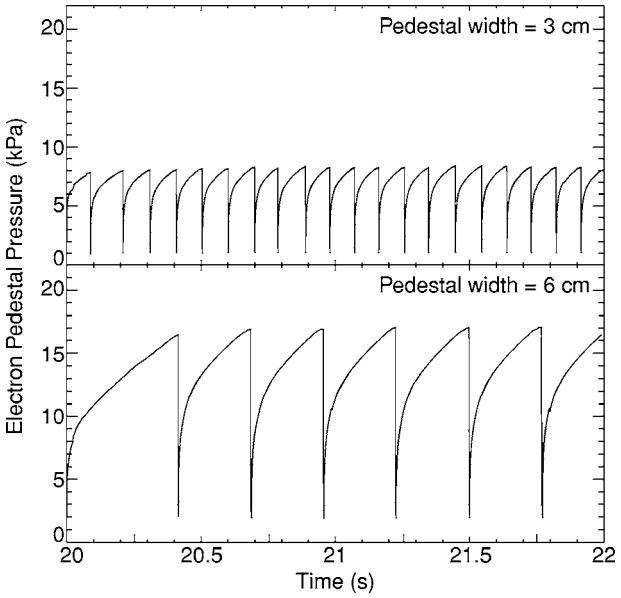

FIG. 7. Electron pedestal pressure vs time for a deuterium discharge using a prescribed pedestal width of 3 cm. (top panel) and a prescribed pedestal width of 6 cm. (bottom panel).

deuterium discharge 43154, a simulation with the pedestal width fixed at 3 cm and another with the pedestal width fixed at 6 cm were carried out. It can be seen in Fig. 7 that the ELM frequency decreases and that the pressure at the top of the pedestal increases substantially as the pedestal width is increased. An analysis of the simulation results presented in this section is presented in Sec. V.

In the baseline simulations considered in this paper, the pedestal width is assumed to be proportional to the ion gyroradius and, consequently, the width increases with isotope mass as in Eq. (3). Many other scalings for the pedestal width depend either directly or indirectly on the isotope mass.[23] In all of the models that include the effect of isotope mass, the pedestal width increases with increasing isotope mass. In a recent model based on the double-Beltrami two-fluid equilibria of Mahajan and Yoshida,[24,25] for example, the width of the pedestal scales like

$$\Delta \propto \rho_i^{2/3} \propto (m_i T_i)^{1/3}. \tag{4}$$

Since the temperature at the top of the pedestal just before each ELM crash is roughly proportional to the pedestal width, an increase in the isotope mass increases both the pedestal width and the pedestal temperature. However, the weaker dependence on isotope mass in Eq. (4), compared with the width proportional to gyroradius in Eq. (3), yields a smaller increase in the pedestal temperature and a smaller decrease in ELM fequency. Interpolation of the simulations that were carried out with a prescribed pedestal width indicates that the increase in the pedestal temperature and the decrease in the ELM frequency using the double-Beltrami model is about half of the corresponding results using a pedestal width proportional to the gyroradius, as the isotope mass is changed from deuterium to tritium. Additional and more refined data is needed before it might be possible to conclude from comparisons with experimental data which of the scalings for the pedestal width is correct.

IV. STABILITY ANALYSIS

The causes of ELM crashes have not been conclusively demonstrated, but it is generally assumed that ELM crashes are triggered by MHD instabilities that arise from the large pressure gradient and current density in the pedestal.[26,27] The stability codes HELENA and MISHKA were employed for the equilibria in the baseline simulations in order to examine ideal MHD stability in the pedestal region just prior an ELM crash. The results obtained with these ideal MHD stability codes were used to adjust the ELM-triggering criteria employed in the JETTO simulations.

To arrive at the numerical value of the critical normalized pressure gradient, α_c, employed in the ballooning stability criterion in the JETTO simulations, the following procedure was employed. As the initial step in an iterative procedure, the value of the normalized pressure gradient used in JETTO is chosen arbitrarily. The equilibrium information from JETTO regarding the state immediately before an ELM crash is used as input to the HELENA code. This equilibrium information consists of the pressure gradient and current density profiles, along with the corresponding shapes of the magnetic surfaces. HELENA refines the equilibrium to produce sufficient resolution for a stability analysis. HELENA and MISHKA are then used with the refined equilibrium to produce a magnetic shear, s, versus normalized pressure gradient, α, stability diagram. The HELENA code evaluates the stability of the infinite-n ballooning modes, and the MISHKA code evaluates the stability of the finite-n ballooning and the low-n kink/peeling modes. The point on the s-α plot that represents the s and α values immediately before an ELM crash in the JETTO simulation is referred to as the "operational point." The value of the normalized critical pressure gradient, α_c, is then adjusted in the JETTO simulations until the operational point is close to the boundary between the stable and unstable region on the s-α stability diagram. It is found that the parameter C in Eq. (2) has a much smaller effect on the ELM trigger than the critical normalized pressure gradient, α_c, which affects the parameter D_M in Eq. (2).

Note that the definition of α used in the HELENA and MISHKA codes is different from the definition of α used in the JETTO code. In the HELENA and MISHKA codes,[28]

$$\alpha \equiv -2(q^2 R/aB^2)dp/d\sqrt{\psi/\psi_{\text{edge}}}, \tag{5}$$

where ψ/ψ_{edge} is the poloidal magnetic flux normalized by its value at the plasma edge (i.e., at the separatrix), whereas, in the JETTO code, α is defined by Eq. (1). Since all of the plasma profile and shape information is passed from the JETTO code to the HELENA and MISHKA codes, and then the α_c used in the JETTO code is adjusted to make the operational point marginally stable according to the HELENA and MISHKA codes, it does not matter that different definitions of α are used in the different codes.

Stability results produced with the HELENA and MISHKA codes are plotted for the tritium discharge in Fig. 8 and for deuterium discharge in Fig. 9. The equilibria used in the

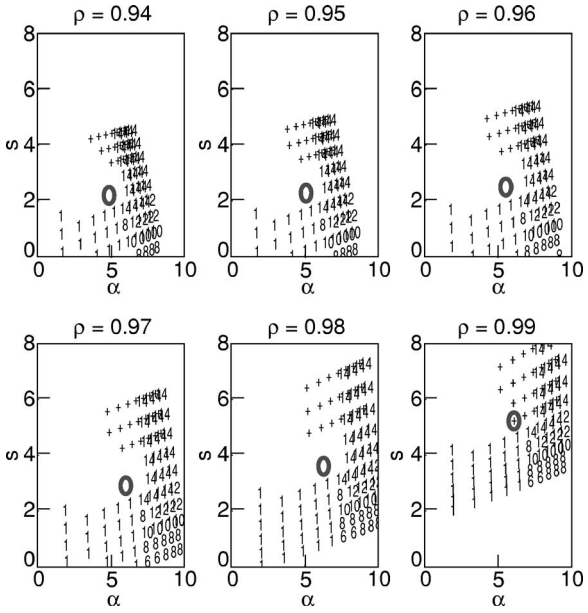

FIG. 8. HELENA and MISHKA stability code results showing the location of unstable modes on a s-α diagram for the JET tritium discharge 43003. The region of instability associated with infinite-n ideal ballooning modes is indicated with crosses. The numbers indicate the most unstable toroidal mode at each location on the s-α plane. Results are shown for flux surfaces from 94% to 99%. The ring denotes the values of s and α given by the JETTO code at that flux surface just prior to an ELM crash.

stability analyses are those obtained from the JETTO code just prior to an ELM crash, using $\alpha_c = 1.65$ in the JETTO code. (Note that the HELENA and MISHKA codes use a normalization for the pressure gradient α that is different from the normalization used in the JETTO code.) The panels in Figs. 8 and 9 show the s-α plots for flux surfaces ranging from the 94% flux surface to the 99% flux surface. These flux surfaces are in the region from the middle of the pedestal to the outer boundary of the pedestal. The criteria for MHD stability are readily achieved in the core, so the core region does not need to be considered in the stability analysis. In Figs. 8 and 9, the crosses indicate locations on the s-α plane that are unstable for infinite-n ballooning modes and the numbers indicate the most unstable toroidal mode number for finite-n ballooning or kink/peeling modes. The blank areas outside of these marked regions are areas of stability. The ring denotes the values of s and α given by the JETTO code at that flux surface just prior to an ELM crash. It can be seen that using JETTO equilibria obtained with $\alpha_c = 1.65$ in both the tritium and deuterium simulations results in an operational point that is close to the marginal stability criterion.

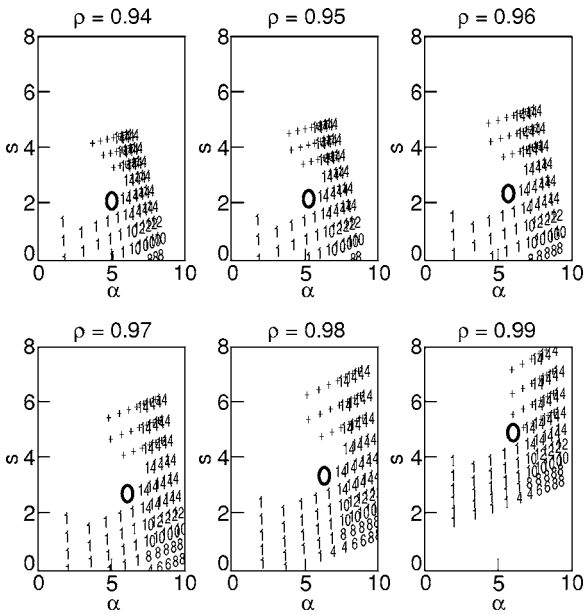

FIG. 9. HELENA and MISHKA stability code results similar to those shown in Fig. 8, but for the deuterium JET discharge, 43154.

The pedestal temperature profile produced by the JETTO simulations are closely approximated by a straight line fit, since the transport in the pedestal between ELM crashes and the heat flux through the pedestal is assumed to be radially uniform. It is generally acknowledged, however, that an ARCTAN fit produces a good approximation to the pedestal temperature profiles observed in experimental data. The curve resulting from an ARCTAN fit can be approximated by a nearly straight line in the central section that flares out with curves at both ends. Hence, a pedestal temperature profile that is approximated by a straight line fit, which is the result of JETTO simulations, is similar to a slightly wider pedestal temperature profile that is approximated by an ARCTAN fit, when both profiles have the same radial slope in the central part of the pedestal. Since the pressure-driven ballooning mode MHD stability of the pedestal is primarily determined by the radial slope of the profile, it is expected that the stability of a pedestal approximated by a straight line fit to the temperature profile will be approximately the same as the stability of a slightly wider pedestal approximated by an ARCTAN fit to the temperature profile (assuming the same density profile for each case). Hence, the scaling of the MHD stability as the pedestal changes in response to the isotope mass is expected to be about the same whether the temperature profile is approximated by a straight line fit or a slightly wider ARCTAN fit.

V. RESULTS AND CONCLUSIONS

It is found that the simulation results for the pressure pedestal height and ELM frequency match the experimentally observed trends as a function of isotope mass only when the width of the pedestal increases with isotope mass. The baseline simulation results, using a pedestal width proportional to the thermal Larmor radius, and the experimental measurements are presented in Table II. Experimental frequency values are given in terms of a range due the inherent ambiguity of ELM frequency, as discussed in Sec. II. It can be seen in Table II that the electron pressure at the top of the pedestal increases moderately with increasing isotope mass and the ELM frequency decreases with increasing isotope mass. The JETTO simulation results exhibit trends that are similar to those observed in the experimental measurements.

The reason that the peak pedestal pressure increases with isotope mass in the simulations can be understood in the following way: It is found that in the deuterium and tritium

TABLE II. A comparison of experimental results and baseline simulation results in which the pedestal width is proportional to the thermal ion Larmor radius.

	JET discharge	Deuterium 43154	Tritium 43003
Electron pedestal	Experiment	10	14
Pressure (kPa)	Simulation	13	14
ELM frequency	Experiment	3–18	2–5
(Hz)	Simulation	7	3

discharges, the ELM crashes are triggered by the criterion for a ballooning mode instability, namely, the normalized pressure gradient α exceeds α_c somewhere within the pedestal region. The critical normalized pressure gradient, α_c, is only very weakly dependent on isotope mass through the effect of the bootstrap current. The pressure gradient is nearly uniform across the pedestal, as seen in Fig. 5. Thus, a wider pedestal results in a higher pressure at the top of the pedestal. Consequently, because the pedestal width increases with isotope mass in the simulations, the pedestal pressure also increases with isotope mass as shown in Table II. The increase in pedestal pressure just before an ELM crash is nearly independent of transport. If the pedestal height were a consequence of neoclassical transport alone, which increases with isotope mass, one would expect the opposite result, namely a decrease in pedestal height with increasing isotope mass.

The reason for the decrease in the ELM frequency with increasing isotope mass in the simulations can be the result of two separate effects. These effects are described below.

The first effect is based on the observation that when more energy is lost during an ELM crash and the heating power is fixed, it takes longer to rebuild the pedestal. As shown in Fig. 5, the pedestal width increases with increasing isotope mass in the baseline simulations. If the pedestal width increases and if the critical normalized pressure gradient for triggering an ELM crash is held fixed, then, as shown in the simulation results presented in Fig. 7, the pedestal pressure approximately doubles with a doubling in the prescribed pedestal width. Consequently, with the larger pedestal width, there is an increase in the energy stored in the pedestal so that a greater energy loss occurs during an ELM crash, as shown in Fig. 10. Therefore, a greater time period is required to reestablish the pedestal with a given heating power.

The second effect is based on the observation that neoclassical transport increases with isotope mass. As a consequence, the pressure gradient and the bootstrap current in the pedestal rebuild more slowly after each ELM crash in simulations with higher isotope mass. Thus, for a given heating power, if thermal transport does increase with isotope mass, the tritium plasma should require a longer regeneration time between ELMs, resulting in a lower ELM frequency than would occur in the deuterium plasma. The dependence of thermal transport on mass is described below.

In the simulations, transport in the pedestal is governed by the ion neoclassical thermal diffusivity, χ_i^{neo}, which has the following approximate dependence:

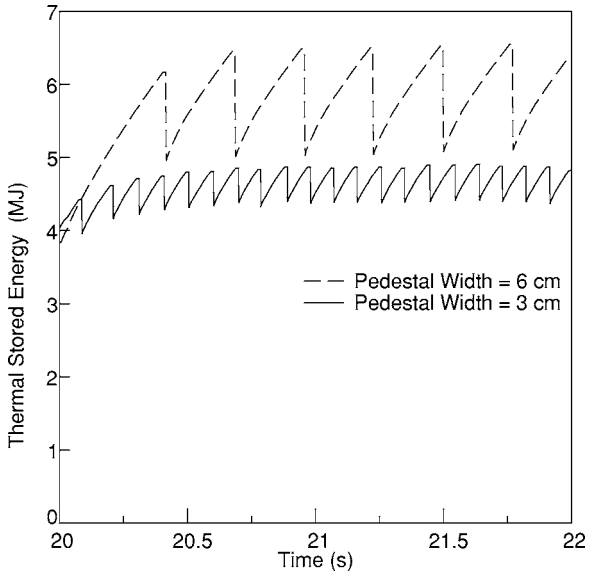

FIG. 10. Thermal stored plasma energy vs time for two different pedestal widths. The upper (dashed) curve corresponds to a pedestal width of 6 cm, while the lower (solid) curve corresponds to a pedestal width of 3 cm.

$$\chi_i^{\text{neo}} \propto \frac{\epsilon^{-3/2} q^2 \rho_i^2}{\tau_i}. \tag{6}$$

Here $\epsilon = r/R$ is the inverse aspect ratio, q is the safety factor, and τ_i is the ion collision time. The Larmor radius is given by

$$\rho_i = (2T_i/m_i)^{1/2}/\omega_{ci}, \tag{7}$$

where $\omega_{ci} = e_i B/m_i$ and m_i is the ion mass. Since ϵ is constant at the top of pedestal, and since $\tau_i \propto \sqrt{m_i} T_i^{3/2}$, then

$$\chi_i^{\text{neo}} \propto \frac{q^2 \rho_i^2}{\tau_i} \propto q^2 m_i^{1/2} T_i^{-1/2}. \tag{8}$$

Hence, the neoclassical ion thermal diffusivity, χ_i^{neo}, increases with isotope mass, m_i, and decreases with ion pedestal temperature, T_i.

The influence of isotope mass on ELM frequency, without including the effect of pedestal temperature, can be observed from the sequence of simulations that were carried out for different isotope masses, but with a choice of fixed pedestal width, as shown in Fig. 6. In these simulations, it is seen that there is only a limited change in electron thermal pressure at the top of the pedestal, but that there is a significant decrease in the ELM frequency with increasing isotope mass. It is likely that this result, at least in part, is due to the increase in ion thermal neoclassical diffusivity with increasing isotope mass, as indicated in Eq. (5). The pressure gradient and the bootstrap current in the pedestal rebuild more slowly after each ELM crash in discharges with higher isotope mass, resulting in a lower ELM frequency, as observed in the simulations and in the experimental data.

In conclusion, it was found that the pedestal width plays a key role in reproducing experimental results in simulations of H-mode discharges with different isotope masses. In the JETTO simulations with the pedestal width increasing with isotope mass, the simulation results reproduce the experi-

mentally observed trends and approximate the measured values for the electron pressure at the top of the pedestal and the ELM frequency. It is found from the HELENA and MISHKA ideal MHD stability codes that the normalized pressure gradient used to trigger ELM crashes remains nearly the same as the isotope mass is increased. The increase in the pedestal pressure with increasing isotope mass just before each ELM crash is a direct consequence of the increase in the pedestal width with increasing isotope mass. The decrease in the ELM frequency with increasing isotope mass is the result of two effects: First, if the pedestal is wider and higher with increasing isotope mass, then more plasma energy is lost during each ELM crash and it takes longer to rebuild the pedestal between ELM crashes. Second, since the thermal diffusivity within the edge barrier increases with increasing isotope mass, it takes longer to increase the pedestal pressure gradient for a given heating power. Consequently, the physical processes are understood in the JETTO simulations, which are consistent with experimental measurements.

ACKNOWLEDGMENTS

This work was funded partly by the U.S. Department of Energy, Contract Number DE-FG02-92-ER-5414, and partly by the United Kingdom Engineering and Physical Sciences Research Council and by the European Communities under the contract of Association between EURATOM and UKAEA. The views and opinions expressed herein do not necessarily reflect those of the European Commission.

[1] ITER Physics Basis Document, Nucl. Fusion **39**, 2137 (1999).
[2] G. Bateman, T. Onjun, and A. H. Kritz, Plasma Phys. Controlled Fusion **45**, 1939 (2003).
[3] J. Kinsey, G. Bateman, T. Onjun *et al.*, Nucl. Fusion **43**, 1845 (2003).
[4] F. Wagner, G. Becker, K. Behringer *et al.*, Phys. Rev. Lett. **49**, 1408 (1982).
[5] A. Loarte, G. Saibene, R. Sartori *et al.*, Phys. Plasmas **11**, 2668 (2004).
[6] G. Saibene, L. D. Horton, R. Sartori *et al.*, Nucl. Fusion **39**, 1133 (1999).
[7] H. Zohm, Plasma Phys. Controlled Fusion **38**, 105 (1996).
[8] T. Onjun, A. H. Kritz, G. Bateman *et al.*, Phys. Plasmas **11**, 1469 (2004).
[9] T. Onjun, A. H. Kritz, G. Bateman *et al.*, Phys. Plasmas **11**, 3006 (2004).
[10] G. Bateman, A. H. Kritz, V. V. Parail *et al.*, Phys. Plasmas **6**, 4607 (1999).
[11] M. Erba, A. Cherubini, V. V. Parail *et al.*, Plasma Phys. Controlled Fusion **39**, 261 (1997).
[12] A. B. Mikhailovskii, G. T. A. Huysmans, S. E. Sharapov, and W. Kerner, Plasma Phys. Controlled Fusion **23**, 844 (1997).
[13] ITPA Scalar Pedestal Database, Version 3.2, http://pc-sql-server.ipp.mpg.de/Peddb/.
[14] J. S. Lönnroth, V. V. Parail, G. Corrigan *et al.*, Plasma Phys. Controlled Fusion **45**, 1689 (2003).
[15] T. Onjun, A. H. Kritz, G. Bateman *et al.*, Phys. Plasmas **12**, 012506 (2005).
[16] W. A. Houlberg, K. C. Shaing, S. P. Hirshman, and M. C. Zarnstorff, Phys. Plasmas **4**, 3230 (1997).
[17] A. H. Kritz, G. Bateman, J. Kinsey, A. Pankin, T. Onjun *et al.*, Comput. Phys. Commun. **164**, 108 (2004).
[18] V. Parail, B. Balet, Y. Baranov *et al.*, Plasma Phys. Controlled Fusion **40**, 805 (1998).
[19] H. R. Wilson, J. W. Connor, A. R. Field *et al.*, Nucl. Fusion **40**, 713 (2000).
[20] W. Hynonen, O. Dumbrajs, A. W. Degeling *et al.*, Plasma Phys. Controlled Fusion **46**, 1409 (2004).
[21] M. Sugihara, Y. Igitkhanov, G. Janeshitz *et al.*, Nucl. Fusion **40**, 1743 (2000).
[22] J. Lönnroth, V. V. Parail, C. Figarella *et al.*, Plasma Phys. Controlled Fusion **46**, A249 (2004).
[23] T. Onjun, G. Bateman, A. H. Kritz, and G. Hammett, Phys. Plasmas **9**, 5018 (2002).
[24] P. Guzdar, S. Mahajan, and Z. Yoshida, Phys. Plasmas **12**, 032502 (2005).
[25] S. Mahajan and Z. Yoshida, Phys. Plasmas **7**, 635 (2000).
[26] J. W. Connor, H. R. Hastie, H. R. Wilson, and R. L. Miller, Phys. Plasmas **5**, 2687 (1998).
[27] P. B. Snyder, H. R. Wilson, J. R. Ferron *et al.*, Phys. Plasmas **9**, 2037 (2002).
[28] G. Huysmans, T. Hender, and B. Alper, Nucl. Fusion **38**, 179 (1998).